International Journal of Computer Mathematics
Vol. 00, No. 00, Month 200x, 1–14

*A*pplication of Domain Decomposition Methods to Indoor Air Flow Simulation

G. LUBE *†, T. KNOPP ‡, R. GRITZKI ♭, M. RÖSLER ♭ and J. SEIFERT ♭

† Mathematics Department, Georg-August University Göttingen, D-37083 Göttingen, Germany
‡ Institute of Aerodynamics and Flow Technology, DLR Göttingen, D-37073 Göttingen, Germany
♭ Institute of Thermodynamics and Building Energy Systems, TU Dresden, D-01602 Dresden, Germany

()

A framework for solving the nonisothermal URANS equations with emphasis on applications to thermal building simulation is prescribed in this paper. Different domain decomposition techniques are used *(i)* for the treatment of boundary layers, *(ii)* for the efficient solution of the arising linear subproblems, and *(iii)* for coupling the indoor air flow field with the ambient. The approach is then applied to exemplary indoor air flow configurations.

Keywords: Domain decomposition; URANS model; stabilized FEM; indoor air flow

AMS Subject Classifications: 65M55; 65N30; 76D05; 76M10; 76R10

1. Introduction

The accurate numerical prediction of indoor-air flows for building configurations of practical relevance requires both a well-resolved flow simulation inside the building and taking into account the effect of the ambient on the indoor-air flow field. The goal of the present paper is to give an overview of recent domain decomposition (DD) techniques for tackling such flow problems. [1]

In the first part of this paper, the focus is on the indoor-air flow as a problem being isolated from the surrounding. Numerical solutions at reasonable computational costs are made amenable by employing two DD methods. First, a modified wall-function method for avoiding a near-wall grid refinement is applied; this method can be interpreted as a DD method with full overlap. Secondly, a non-overlapping DD method (iteration-by-subdomains) is used, which allows a parallel solution of linearized problems of Oseen and advection-diffusion-reaction type.

In the second part, two other DD methods are described, which are used in order to improve the physics involved in the computational model. For getting more realistic boundary conditions at openings of the flow domain, the computational domain is extended by a suitable ambient surrounding. Inflow and outflow are then handled by the iteration-of-subdomains method. Finally, realistic predictions require an active coupling between the interior of the building and its surrounding. This gives rise to a hybrid DD method which is performed by coupling the flow solver with thermal building simulation.

2. Governing equations for buoyancy driven incompressible flow

Consider the non-dimensional incompressible, non-isothermal, unsteady Reynolds-averaged Navier-Stokes (URANS) equations with a turbulence model to be specified later [1]. Buoyancy forces are modeled using

*Corresponding author. Email: lube@math.uni.goettingen.de

[1]The paper is based on a keynote lecture given by the first author during the International Conference DCABES-05 at the University of Greenwich.

International Journal of Computer Mathematics
ISSN 0020-7160 print/ISSN 1029-0265 online © 200x Taylor & Francis
http://www.tandf.co.uk/journals
DOI: 10.1080/0020716YYxxxxxxxx

the Boussinesq approximation. In a bounded domain $\Omega \subset \mathbf{R}^d$, $d = 2, 3$, velocity $\mathbf{u}$, pressure p, and temperature θ are solutions of the coupled system

$$\begin{aligned} \partial_t \mathbf{u} - \nabla \cdot (2\nu_e \mathbf{S}(\mathbf{u})) + (\mathbf{u} \cdot \nabla)\mathbf{u} + \nabla p &= -\beta\theta\mathbf{g}, \\ \nabla \cdot \mathbf{u} &= 0, \\ \partial_t \theta + (\mathbf{u} \cdot \nabla)\theta - \nabla \cdot (a_e \nabla\theta) &= c_p^{-1}\dot{q}^V \end{aligned} \tag{1}$$

with $\mathbf{S}(\mathbf{u}) := \frac{1}{2}(\nabla\mathbf{u} + \nabla\mathbf{u}^T)$, isobaric volume expansion coefficient β, gravitational acceleration $\mathbf{g}$, volumetric heat source $\dot{q}^V$, and specific heat capacity (at constant pressure) c_p. Effective viscosities $\nu_e = \nu + \nu_t$ and $a_e = a + a_t$ are introduced with kinematic viscosity ν, turbulent viscosity ν_t, thermal diffusivity $a = \nu/Pr$ and turbulent thermal diffusivity $a_t = \nu_t/Pr_t$ with Prandtl numbers $Pr = 0.7$ and $Pr_t = 0.9$. The non-constant ν_t and a_t model turbulent effects and depend on the chosen turbulence model. Other passive scalar fields like age of the air or concentration of pollutants can be easily appended to model (1), see [5].

Depending on the sign of $\mathbf{u} \cdot \mathbf{n}$, the boundary $\partial\Omega$ is divided into wall zones $\Gamma_0 \equiv \Gamma_W$, inlet zones Γ_- and outlet zones Γ_+. Boundary conditions are imposed as

$$\sigma(\mathbf{u}, p)\mathbf{n} = \tau_n \mathbf{n} \ \text{ on } \Gamma_- \cup \Gamma_+ \,, \qquad \mathbf{u} = \mathbf{0} \ \text{ on } \Gamma_0 \tag{2}$$

with $\sigma(\mathbf{u}, p) = 2\nu_e \mathbf{S}(\mathbf{u}) - p\mathbf{I}$. For θ one requires

$$\theta = \theta_{in} \ \text{ on } \Gamma_- \,, \quad a_e \nabla\theta \cdot \mathbf{n} = 0 \ \text{ on } \Gamma_+ \,, \quad \theta = \theta_w \ \text{ on } \Gamma_0. \tag{3}$$

The in- and outflow conditions in (2) are suitable for the specification of natural ventilation problems. In Section 5 an alternative approach to boundary conditions on $\Gamma_- \cup \Gamma_+$ is considered using a non-overlapping DD method.

The time discretization is performed, for simplicity, with the BDF(1) scheme with $\partial_t \phi \approx \frac{\phi - \phi_{old}}{\delta t}$ for some variable ϕ. This leads to a sequence of coupled nonlinear problems to be solved within each time step.

3. Domain decomposition with full overlap for boundary layers

For brevity, it is assumed here that $\partial\Omega = \Gamma_0 \equiv \Gamma_W$; for the general case see [5]. Near Γ_W, velocity $\mathbf{u}$ and temperature θ exhibit strong gradients. Fig. 1 (left) shows a typical near-wall profile for the streamwise component of $\mathbf{u}$ for the flow along a heated vertical wall. In order to circumvent an expensive anisotropic grid refinement in the near-wall region, an overlapping DD approach is applied, see Fig. 1 (right).

The global problem in Ω reads

$$\begin{aligned} -\nabla \cdot (\nu_e \nabla\mathbf{u}) + (\mathbf{u} \cdot \nabla)\mathbf{u} + (\delta t)^{-1}\mathbf{u} + \nabla p &= -\beta\theta\mathbf{g} + (\delta t)^{-1}\mathbf{u}_{old} \\ \nabla \cdot \mathbf{u} &= 0 \\ -\nabla \cdot (a_e \nabla\theta) + (\mathbf{u} \cdot \nabla)\theta + (\delta t)^{-1}\theta &= c_p^{-1}\dot{q}^V + (\delta t)^{-1}\theta_{old} \end{aligned} \tag{4}$$

with modified boundary conditions on Γ_W

$$\mathbf{u} \cdot \mathbf{n} = 0 \,, \qquad (\mathbf{I} - \mathbf{n} \otimes \mathbf{n})\sigma(\mathbf{u}, p)\mathbf{n} = \tau_t(\mathbf{u}, \mathbf{u}^L, \theta^L) \tag{5}$$

$$a_e \nabla\theta \cdot \mathbf{n} = c_p^{-1}\dot{q}(\mathbf{u}^L, \theta^L). \tag{6}$$

The boundary data τ_t, $\dot{q}$ at Γ_W are taken from the boundary layer solution $(\mathbf{u}^L, p^L, \theta^L)$ of (4) in the region

Ω_δ (see Fig. 1 right) with boundary conditions

$$\mathbf{u}^L \;=\; \mathbf{0},\;\; \theta^L \;=\; \theta_w \quad \text{on } \Gamma_W; \qquad \mathbf{u}^L \;=\; \mathbf{u},\;\; \theta^L \;=\; \theta \quad \text{on } \Gamma_\delta. \tag{7}$$

Now the turbulent viscosity ν_t and the data $\tau_t,\ \dot{q}$ in (5)-(6) are specified. Moreover, the boundary layer model is simplified:

As the global turbulence model in Ω one can select a standard one- or two-equation model (e.g. Spalart-Allmaras, $k-\omega$). Here, as a reasonable choice for indoor-air flow, the $k-\epsilon$ model with $\nu_t = c_\mu k^2/\epsilon,\ c_\mu = 0.09$ is used. The turbulent kinetic energy k and dissipation ϵ are semidiscrete solutions of

$$\begin{aligned} -\nabla\cdot(\nu_k\nabla k) + (\mathbf{u}\cdot\nabla)k + (\delta t)^{-1}k &= P_k + G - \epsilon + (\delta t)^{-1}k_{old} \\ -\nabla\cdot(\nu_\epsilon\nabla\epsilon) + (\mathbf{u}\cdot\nabla)\epsilon + (\delta t)^{-1}\epsilon + C_2\epsilon^2 k^{-1} &= C_1\epsilon k^{-1}(P_k+G) + (\delta t)^{-1}\epsilon_{old} \end{aligned} \tag{8}$$

with effective viscosities $\nu_k = \nu + \nu_t/Pr_k, \nu_\epsilon = \nu + \nu_t/Pr_\epsilon$, production and buoyancy terms $P_k = 2\nu_t|\mathbf{S}(\mathbf{u})|^2$, $G = \beta a_t \mathbf{g}\cdot\nabla\theta$ and constants $C_1 = 1.44, C_2 = 1.92, Pr_k = 1.0, Pr_\epsilon = 1.3$. The $k-\epsilon$ equations (8) are solved in $\Omega\backslash\Omega_\delta$ with the boundary conditions $k = c_\mu^{-1/2}U_*^2$, $\epsilon = U_*^3/(\kappa y)$ on Γ_δ with $\kappa = 0.41$ and $U_* = |\tau_t|^{1/2}$.

A modified wall-function approach for a simplified boundary layer model in Ω_δ is applied. Denote x, y, z the streamwise, wall-normal and spanwise direction resp. in a wall-fitted coordinate system, see Fig. 1 (left). According to Prandtl's boundary layer theory, we approximate (4)-(7) in Ω_δ by a system of coupled ODEs

$$\begin{aligned} -\frac{d}{dy}\left(\nu_e^L\frac{du_x^L}{dy}\right) \;&=\; -\beta\theta^L g_x, \quad -\frac{d}{dy}\left(a_e^L\frac{d\theta^L}{dy}\right) \;=\; 0, \\ u_x^L|_{y=0} \;&=\; 0\ , \qquad\qquad \theta^L|_{y=0} \;=\; \theta_w, \end{aligned} \tag{9}$$

with the streamwise component g_x of $\mathbf{g}$ and with matching conditions

$$u_x^L|_{y=y_\delta} = u_x(y_\delta), \qquad \theta^L|_{y=y_\delta} = \theta(y_\delta). \tag{10}$$

For physical reasons, the following algebraic effective viscosities in Ω_δ

$$\nu_e^L = \nu\max\left(1; \frac{Re}{Re_{min}}\right), \quad a_e^L = \frac{\nu}{Pr}\max\left(1; \frac{Pr}{Pr_t^L}\frac{Re}{Re_{min}}\right) \tag{11}$$

are taken with $Re = |\mathbf{u}^L|y/\nu$ and $Pr_t^L = 1.16$. Effects of thermal stratification in the boundary layer are of prime importance. They are taken into account via the empirical formula [10]

$$Re_{min} = \min\Big(\ 20.0e^{-25.0\frac{\dot{q}Pr}{U_*^4}\frac{\nu}{\mathbf{g}\cdot\mathbf{n}}}\ ;\ 70.0\Big). \tag{12}$$

Now the model is decoupled and linearized within each time step:

(A) First update ν_t, a_t. Then update τ_t, $\dot{q}$: Given u_x, θ on Γ_δ from the previous iteration cycle, replace the boundary condition (10) with

$$\nu_e^L\frac{du_x^L}{dy}|_{y=0} = R, \qquad a_e^L\frac{d\theta^L}{dy}|_{y=0} = S. \tag{13}$$

Solve the initial value problem (9),(13) with (11),(12) using a shooting method for (R, S) on a layer-adapted mesh until the conditions (10) are fulfilled. Then find the r.h.s. $\tau_t = -U_*^2\mathbf{u}/|\mathbf{u}|$ and $\dot{q}$ in (5),(6) by setting $U_*^2 = R$ and $\dot{q} = c_p S$.

(B) Solve the global problem (4)-(6) and, if the k-ϵ model is used, additionally (8), using an iterative block Gauss-Seidel method, see [5, 19].
(C) Goto (A) if some stopping-criterion is not fulfilled. Otherwise goto next time step.

The iteration within each time step can be seen as an overlapping DD method. Moreover, the $k-\epsilon$ model can be replaced by another eddy-viscosity based model. The v^2-f model which circumvents some drawbacks of the $k-\epsilon$ model is currently under investigation. First reasonable results for the isothemal flow in a three-dimensional channel are given in [6]. For recent progress with adaptive wall functions in the isothermal case, see [3, 4].

4. Domain decomposition of linearized problems

Two basic problems are to solve in step (B). The first is the linearized Navier-Stokes problem of Oseen-type with positive reaction term and variable viscosity (skipping the restriction $\partial\Omega = \Gamma_0$ in the sequel):

$$\begin{aligned} L_O(\mathbf{a},\mathbf{u},p) \equiv -\nabla\cdot(2\nu\mathbf{S}(\mathbf{u})) + (\mathbf{a}\cdot\nabla)\mathbf{u} + c\mathbf{u} + \nabla p &= \mathbf{f} \quad \text{in } \Omega \\ \nabla\cdot\mathbf{u} &= 0 \quad \text{in } \Omega \\ \sigma(\mathbf{u},p)\mathbf{n} &= \tau_n\mathbf{n} \quad \text{on } \Gamma_-\cup\Gamma_+ \\ (\mathbf{I}-\mathbf{n}\otimes\mathbf{n})\sigma(\mathbf{u},p)\mathbf{n} = \tau_t, \qquad \mathbf{u}\cdot\mathbf{n} &= 0 \quad \text{on } \Gamma_0. \end{aligned} \tag{14}$$

Secondly, the linearized equations for θ, k and ϵ are advection-diffusion-reaction (ADR) problems in $\tilde\Omega = \Omega$ or $\tilde\Omega = \Omega\setminus\Omega_\delta$ with variable viscosity of the form:

$$\begin{aligned} L_{ADR}u \equiv -\nabla\cdot(\nu\nabla u) + (\mathbf{a}\cdot\nabla)u + cu &= f \quad \text{in } \tilde\Omega \\ u &= g \quad \text{on } \tilde\Gamma_D \\ \nu\nabla u\cdot\mathbf{n} &= h \quad \text{on } \tilde\Gamma_N. \end{aligned} \tag{15}$$

For the finite element discretization of (14)-(15), admissible triangulations $\mathcal{T}_h = \{K\}$ of the domain Ω together with discrete subspaces of globally continuous and piecewise polynomial ansatz and test functions are considered.

It is well-known that the standard Galerkin FEM for the Oseen problem (14) with an equal-order ansatz for velocity and pressure does not pass the discrete inf-sup condition. Therefore a pressure stabilization (PSPG) together with divergence and SUPG stabilization is applied [5]. Moreover, the Galerkin-FEM with SUPG-stabilization for the ADR-problem (15) is used together with a (nonlinear) shock-capturing method , see [5].

The development of efficient domain decomposition methods for such linear problems is a matter of ongoing research, see, e.g., [13, 17]. Here, an approach (with a reasonable theoretical background) is preferred which is easy to implement. More precisely, a parallelized solution of the linearized problems (14), (15) is permitted by applying an iterative substructuring method which couples the subdomain problems via Robin-type transmission conditions [5]. Consider a non-overlapping partition of Ω into N convex, polyhedral subdomains being aligned with the FE mesh, i.e.

$$\bar\Omega = \bar\Omega_1\cup\cdots\cup\bar\Omega_N, \quad \Omega_k\cap\Omega_j = \emptyset \quad \forall k\neq j\ , \quad \forall K\in\mathcal{T}_h\ \exists k:\ K\subset\Omega_k.$$

Furthermore, set $\Gamma_k := \partial\Omega_k\backslash\partial\Omega$, $\Gamma_{jk} := \partial\Omega_j\cap\partial\Omega_k$, $j\neq k$, where $\Gamma_{kj} = \Gamma_{jk}$. Assume, for simplicity, that the partition is stripwise.

The DD method is defined for the Oseen problem (14) as follows: for given $(\mathbf{u}_k^n, p_k^n)$ from step n on each Ω_k, seek (in parallel) for $(\mathbf{u}_k^{n+1}, p_k^{n+1})$

$$L_O(\mathbf{a},\mathbf{u}_k^{n+1},p_k^{n+1}) = \mathbf{f} \qquad \text{in } \Omega_k$$

$$\begin{aligned} \nabla \cdot \mathbf{u}_k^{n+1} &= 0 \qquad \text{in } \Omega_k \\ \sigma(\mathbf{u}_k^{n+1}, p_k^{n+1})\mathbf{n}_k &= \tau_n \mathbf{n}_k \ \text{ on } \partial\Omega_k \cap (\Gamma_- \cup \Gamma_+) \\ \pi_{t,k}\sigma(\mathbf{u}_k^{n+1}, p_k^{n+1})\mathbf{n}_k &= \tau_t, \quad \mathbf{u}_k^{n+1} \cdot \mathbf{n}_k = 0 \qquad \text{on } \partial\Omega_k \cap \Gamma_0 \end{aligned}$$

with $\pi_{t,k} := I - \mathbf{n}_k \otimes \mathbf{n}_k$, together with the interface conditions

$$\Phi_k(\mathbf{u}_k^{n+1}, p_k^{n+1}) = \ \vartheta\Phi_k(\mathbf{u}_j^n, p_j^n) + (1-\vartheta)\Phi_k(\mathbf{u}_k^n, p_k^n) \ \text{ on } \Gamma_{jk},\ j = 1, \ldots, N,\ j \neq k.$$

$\vartheta \in (0, 1]$ is a relaxation parameter. The interface function is given by

$$\Phi_k(\mathbf{u}, p) = \sigma(\mathbf{u}, p) \cdot \mathbf{n}_k + (-\frac{1}{2}\mathbf{a} \cdot \mathbf{n}_k + z_k)\mathbf{u} \tag{16}$$

with acceleration parameters z_k.

For the ADR-problem (15) the DD method reads: for given u_k^n from iteration step n on each Ω_k, seek (in parallel) for u_k^{n+1}

$$\begin{aligned} L_{ADR}u_k^{n+1} &= f \quad \text{in } \Omega_k \\ u_k^{n+1} &= 0 \quad \text{on } \Gamma_D \cap \partial\Omega_k \\ \nu\nabla u_k^{n+1} \cdot \mathbf{n}_k &= h \quad \text{on } \Gamma_N \cap \partial\Omega_k \end{aligned}$$

together with the interface conditions

$$\Phi_k(u_k^{n+1}) = \vartheta\Phi_k(u_j^n) + (1-\vartheta)\Phi_k(u_k^n) \quad \text{on } \Gamma_{jk},\ j = 1, \ldots, N,\ j \neq k$$

with a relaxation parameter $\vartheta \in (0, 1]$. The interface function is specified as

$$\Phi_k(u) = \nu\nabla u \cdot \mathbf{n}_k + (-\frac{1}{2}\mathbf{a} \cdot \mathbf{n}_k + z_k)u. \tag{17}$$

For the formulation of the DD method on the discrete level, see [5].

A basic advantage for the practical implementation of the method with Robin-type interface conditions is that the algorithm can be split into a parallel computation step for $(\mathbf{u}_k^{n+1}, p_k^{n+1})$ and u_k^{n+1}, respectively, and a parallel communication step for an update of the Lagrangian multipliers of the interface conditions.

The algorithms for both linear problems are well-posed if $z_k = z_j > 0$. The sequences $\{\mathbf{u}_k^n\}_n$ for the velocity in the Oseen problem and $\{u_k^n\}_n$, $k = 1, ..., N$ for the scalar field in the ADR-problem converge strongly to the restrictions of the global discrete solutions to Ω_k w.r.t. stabilized energy norms [8, 11] and [7], respectively.

Convergence rates are not available in the a-priori estimate. Nevertheless, appropriate a-posteriori estimates allow to control the convergence on subdomains via jumps of the DD solutions across the interface. This technique has been developed for the ADR-problem in [7] and extended, e.g., in [8, 11] to the Oseen problem. In Fig. 2, it is shown for a typical ADR problem that the error in the energy norm on the subdomains is efficiently controlled by the interface error. Moreover, we observe that an optimization of the acceleration parameter z_k is in order. Indeed, besides the a-posteriori estimate provides the principal design of the acceleration parameter

$$z_k = \frac{1}{2}|\mathbf{a} \cdot \mathbf{n}_k| + R_k(L_k, \nu, c, \mathbf{a}), \quad L_k \in \{h, H_k\}, \quad H_k = \text{diam}(\Omega_k), \tag{18}$$

with

$$R_k \sim \frac{\nu}{H_k}\sqrt{\frac{H_k}{L_k}}\left[1 + H_k\sqrt{\frac{c}{\nu}} + \min\left(\frac{\|\mathbf{a}\|_{max}}{\sqrt{\nu c}}; \frac{H\|\mathbf{a}\|_{max}}{\nu}\right)\right]; \tag{19}$$

for details see [7] and [8]. Fig. 2 gives some impression of the considerable acceleration of convergence for the choice $L_k = H_k$. In particular, the value of $z_k = 0.1$ corresponds to the optimized parameter. Additional numerical experiments can be found in [7, 8, 11] and in references therein.

The relaxation parameter ϑ in the interface conditions may considerably influence the convergence of the DD iteration. This is the case, in particular, if the flow field $\mathbf{a}$ is tangential to an interface. Moreover, the convergence of the pressure in the Oseen problem can be accelerated in certain cases. Generally, a slight under-relaxation with $\vartheta \sim 0.9$ can be recommended.

In a recent paper, see [9], it has been observed for the ADR-problem that an additional convergence acceleration of the DD method is possible using a cyclic two-level DD-approach with z_k^1 related to $L_k = H_k$ and z_k^2 related to $L_k = h$. In Fig. 3, the standard case with $L_k = H_k$ (left) is compared to the two-level approach for a typical ADR-problem. It might be only of theoretical interest that the error between the discrete DD solution and the discrete solution without DDM can be driven to machine accuracy for the new variant. More remarkably is that already for the first iterations the convergence can be accelerated.

5. Domain decomposition approach for coupling the interior flow with radiative heat transfer and ambient

The proposed approach has been implemented in the research code ParallelNS. A stabilized finite element discretization is performed with globally continuous and piecewise linear ansatz and test functions for the unknowns $\mathbf{u}, p, \theta, k, \epsilon$ on unstructured tetrahedral (resp. triangular) meshes in 3D (resp. 2D). A BDF-scheme is used for the semidiscretization in time.

Parallelization is accomplished using a master/slave paradigm in a PVM configuration. Computations were performed on either a cluster of four Compaq Professional Workstations XP1000 (667 MHz) connected by Ethernet or on Siemens Celsius machines with two Opteron processors (1.8 GHz) and 6 GB RAM. A multitude of numerical results indicate that the approach is suitable for the parallel computation of indoor-air flows in the coarse-granular case as no coarse grid solver is used so far.

The approach is applied at Dresden University of Technology as an analysis tool for the design and investigation of heating and ventilation systems, see [14]. Emphasis is both on hygienic and on energetic aspects of the indoor-air climate. Regarding the hygienic point of view, the distribution of the local age of the air is of prime importance. An additional ADR equation modelling this quantity is included in the method in a straightforward way, see Section 2.

5.1. *Full coupling with the ambient surrounding.*

In the first simulation, the natural ventilation flow in a cavity with openings of size $h/b = 0.3\text{m}/1.5\text{m}$ and a heating rod with $\dot{Q} = 300\text{W}$ is considered, see Fig. 4. The initial temperature distribution in the cavity and in the external domain is homogeneous with $\theta_{L,in}|_{t=0} = 28.5^o\text{C}$ and $\theta_{L,ex}|_{t=0} = 27.9^o\text{C}$. This temperature difference and the heating rod induce a buoyancy-driven fluid motion which simulates a displacement ventilation with completely opened windows. The Rayleigh number $Ra = 2.0184 \cdot 10^{10}$ corresponds to a turbulent flow. The method is assessed by reference with an experimental configuration and data, see [2].

The simulation of this flow requires the application of two additional DD methods. Firstly, the computational domain Ω is enlarged as sketched in Figure 4. In order to get physically more correct data at the inflow of the cavity Ω_{int}, a suitable ambient surrounding Ω_{ext} is also taken into account, so that $\overline{\Omega} = \overline{\Omega}_{int} \cup \overline{\Omega}_{ext}$. The inflow and outflow conditions at the openings are modified as follows since the fields τ_n in (2) and θ_{in} in (3) are usually not known. Instead, the application of the interface conditions of the DD method, as presented in Section 3 provides a natural treatment of the inflow and outflow at the openings. For a similar approach in case of wind-loads, see [5]. Suitable boundary conditions have to be imposed on

$\partial\Omega$. For natural ventilation problems, the first condition in (2) with $\tau_n = 0$ for $\mathbf{u}$ and condition (3) for θ with $\theta_{in} = \theta_{ext}$ are imposed.

Secondly, an active coupling between the flow inside the cavity and the ambient is required, which is performed using a special version of the building simulation tool TRNSYS (TRNSYS-TUD), see [18] and [12]. This requires the thermal coupling with an additional domain, the envelope of the cavity denoted by Ω_W , see Figure 4. The flow simulation requires as an input the wall temperature θ_w in boundary condition 3. This is provided by building simulation as a result from a balance of conduction, radiation and convection in the cavity including walls.

For this purpose, the building simulation tool has to determine *(i)* the radiative heat transfer inside the room, *(ii)* convective heat transfer across the boundary layer, and *(iii)* diffusive heat transfer across the walls due to the temperature gradient between the inner wall temperature and the ambient temperature by Fourier's law.

Of major importance is an accurate prediction of *(ii)*. We consider the coefficient of convective heat transfer $h_{c,i}$ at the discrete wall-element i. Then $h_{c,i}$ is given by Newton's cooling law

$$h_{c,i} \;=\; -\frac{\dot{q}_i}{\theta_{w,i} - \theta_{\delta,i}}$$

where $\dot{q}_i$ is given by the wall-function method from the flow-solver, and $\theta_{w,i}$ and $\theta_{\delta,i}$ are the temperature at Γ_0 resp. at Γ_δ, which are all interpolated appropriately to the mesh applied for thermal building simulation. From these data, the building simulation tool computes the new wall temperatures $\theta_{w,i}$ which are then interpolated onto the finer FEM mesh for the next flow solver step. This coupling between ParallelNS and TRNSYS-TUD is done once each time step. Details of this coupling can be found in [15].

Regarding the FEM simulation, the application of the wall-function method allows to use a relatively coarse unstructured tetrahedral mesh with about 121.000 elements in the internal domain without resolving the near-wall region. The first grid points above the wall reside at $y_\delta = 0.05$m, which is slightly beyond the velocity maximum in the free-convection boundary layer in Fig. 1 (left). Equations (9)-(12) are solved in Ω_δ on an auxiliary grid with 20 equidistant grid nodes in wall-normal direction.

The quasi-stationary flow field is shown in Fig.5 in three cross-sections ($x = 0.465$m, $x = 1.215$m and $x = 1.965$m). Concerning the accuracy of the method, Fig.6 shows a comparison of the temperature distribution $\theta = \theta(z)$ measured and calculated at $x = 1.215\text{m}, y = 1.10\text{m}$ over a long-time period of 7200s. A visible difference appears at the early time $t = 180$s during the transient stage of the flow, which might be due some flaws of the $k - \epsilon$ model for application to transient flows and due to the low-order time-discretisation scheme. The quasi-steady solution is in reasonably well agreement with the experimental data.

5.2. *Indoor-air flow in an atrium*

Consider now the numerical simulation of air-flow conditions in an atrium (with cafeteria) of size $22m \times 22.5m \times 17.2m$, cf. Fig. 7. The boundary conditions are taken from a thermal simulation of the surrounding rooms of the building using TRNSYS-TUD. A domain decomposition into three subdomains is performed. The finite element mesh consists of approximately 1.2×10^6 tetrahedra, the resulting nonlinear algebraic systems (per time step) have approximately 2×10^6 unknowns. This leads to storage requirements of about 2 GB.

The numerical simulation was performed under winter conditions over a period of two hours real time. The CPU time on the Opteron machine with two processors and three subdomains was about 70 hours. A third processor would reduce the CPU time to less then 40 hours.

The former situation was characterized by unpleasant air flow and temperature conditions caused by the curved glass roof. In particular, the maximum velocity in the occupied zone reached unacceptable values. An improvement of the air flow conditions was possible with an additional heating system below the roof which yields a reduction of maximum velocity to acceptable values.

The resulting temperature field is presented in Fig. 8. The implementation of the additional heating

system under the roof gives an acceptable temperature distribution in all relevant zones of the atrium. For some details of the flow field, see Fig. 9.

6. Summary

In this paper, an approach is presented based on a combination of different domain decomposition techniques for the reliable and efficient simulation of indoor air flow problems coupled with radiative heat transfer and the ambient. The method has been applied successfully to a benchmark like problem and to an exemplary complex building configuration. The framework is used as an analysis tool for the design and investigation of heating and ventilation systems. Ongoing research is devoted to the development of an optimization tool for indoor air flows using the present framework.

References

[1] P.A. Durbin, B.A. Petterson Reif: Statistical Theory and Modelling for Turbulent Flows, John Wiley and Sons, Chichester, 2001.
[2] V. Haslavsky, J. Tanny, M. Teitel: Interaction between the mixing and displacement modes in a naturally ventilated enclosure, *Building and Environment*, in press, 2005
[3] G. Kalitzin, G. Medic, G. Iaccarino, P. Durbin: Near-wall behavior of RANS turbulence models and implications for wall function, *J. Comp. Phys.*, **2**04, 265-291. 2005.
[4] T. Knopp, Th. Alrutz, D. Schwamborn: On grid-indenpendence of RANS solutions of separated flows using universal wall-functions with near-wall grid adaption, accepted for J. Comput. Phys. 2006.
[5] T. Knopp, G. Lube, R. Gritzki, M. Rösler: A near-wall strategy for buoyancy-affected turbulent flows using stabilized FEM with applications to indoor air flow simulation, *Comput. Meth. Appl. Mech. Engrg.*, 194 (2005) 3797-3816, 2005.
[6] G. Lube, T. Knopp, R. Gritzki: Stabilized FEM with anisotropic mesh refinement for the Oseen problem, in: Proceedings ENUMATH 2005, Springer 2006, pp. 799-807
[7] G. Lube, L. Müller, F. C. Otto: A non-overlapping domain decomposition method for the advection-diffusion problem, *Computing*, **6**4, 49-68, 2000.
[8] G. Lube, L. Müller, F. C. Otto: A non-overlapping DD method for stabilized finite element approximations of the Oseen equations, *J. Comp. Appl. Math.*, **1**32, 211-236, 2001.
[9] G. Lube, T. Knopp, G. Rapin: Acceleration of an iterative substructuring method for singularly perturbed elliptic problems, in: Proceedings 15. Int. Conf. Domain Decomposition Methods, Berlin 2003, 267-274.
[10] K. P. Neitzke: Experimentelle Untersuchung und numerische Modellierung von wandnahen thermischen Auftriebsströmungen, PhD Thesis, TU Dresden, 1999.
[11] F.C. Otto, G. Lube, H. Müller: An iterative substructuring method for div-stable finite element approximations of the Oseen problem, Computing 67 (2001) 91-117.
[12] A. Perschk: Gebäude-Anlagen-Simulation unter Berücksichtigung der hygrischen Prozesse in den Gebäudewänden, PhD Thesis, TU Dresden, 2001.
[13] A. Quarteroni, A. Valli: Domain Decomposition Methods for Partial Differential Equations, Oxford Science Publications, 1999.
[14] W. Richter: Handbuch der thermischen Behaglichkeit -Heizperiode-, Wirtschaftsverlag NW, Bremerhaven, 2003.
[15] J. Seifert: Zum Einfluss von Luftströmungen auf die thermischen und aerodynamischen Verhältnisse in und an Gebäuden, PhD Thesis, TU Dresden, 2005.
[16] R. Siegel, J. Howell: Thermal Radiation Heat Transfer, 4th ed., Taylor and Francis-Hemisphere, Washington.
[17] A. Toselli, O. Widlund: Domain Decomposition Methods: Algorithms and Theory, Springer, Berlin, 2004.
[18] TRNSYS a transient system simulation programm, User Manual, Transsolar Energietechnik GmbH Stuttgart.
[19] S. Turek, D. Kuzmin: Algebraic flux correction III. Incompressible flow problems, in: D. Kuzmin, R. Löhner, S. Turek (eds), *Flux-Corrected Transport: Principles, Algorithms and Applications*, Springer, 2005, 251-296.

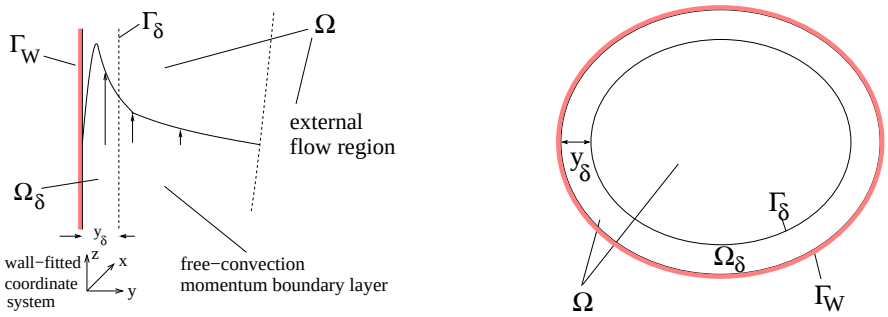

Figure 1. Domain decomposition in the boundary layer region.

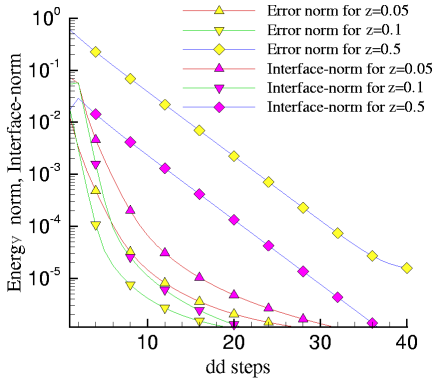

Figure 2. Reliability of the a posteriori estimate for $\nu = 10^{-2}$ and $h = \frac{1}{128}$

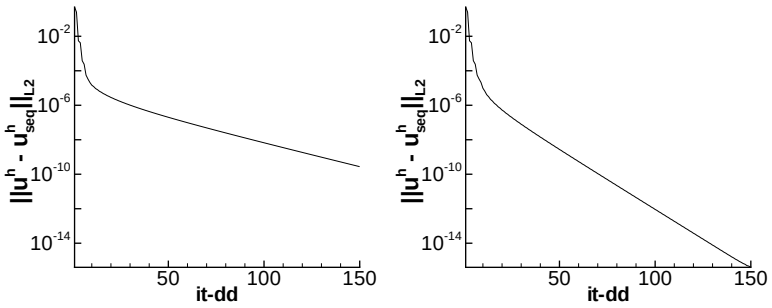

Figure 3. Error reduction for standard case $L_k = H_k$ (left) and two-level case (right)

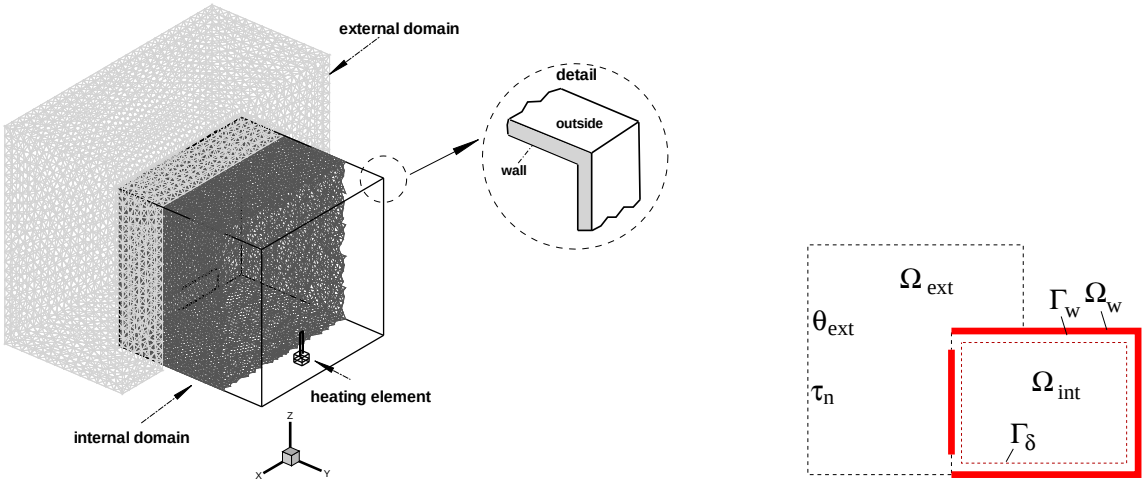

Figure 4. Coupling of CFD solver with thermal building simulation. Left: DDM for improved inflow/outflow at openings and interaction with walls (detail). Right: Four domains of a coupled simulation of natural ventilation

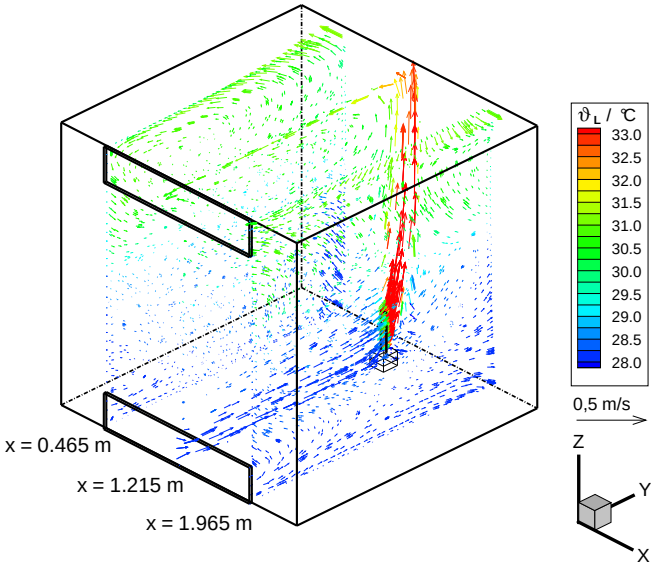

Figure 5. Prediction for θ at three cross-sections with $x = 0.465\text{m}/1.215\text{m}/1.965\text{m}$.

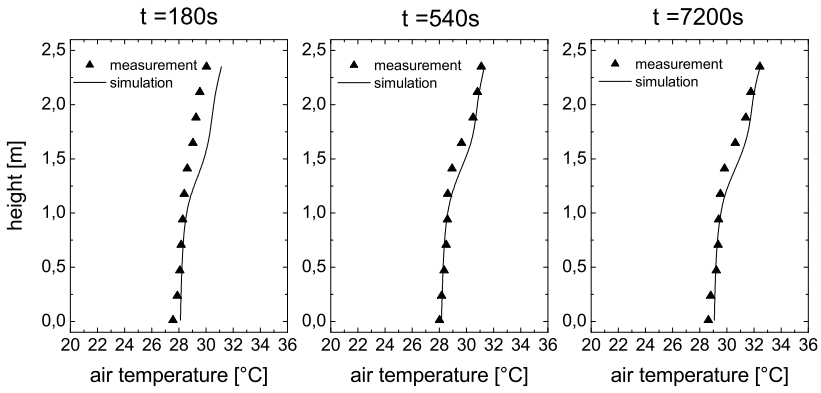

Figure 6. Comparison of temperature $\theta = \theta(z)$ measured and calculated at $x = 1.215$ m, $y = 1.10$ m and $t = 180$ s/540 s/7200 s

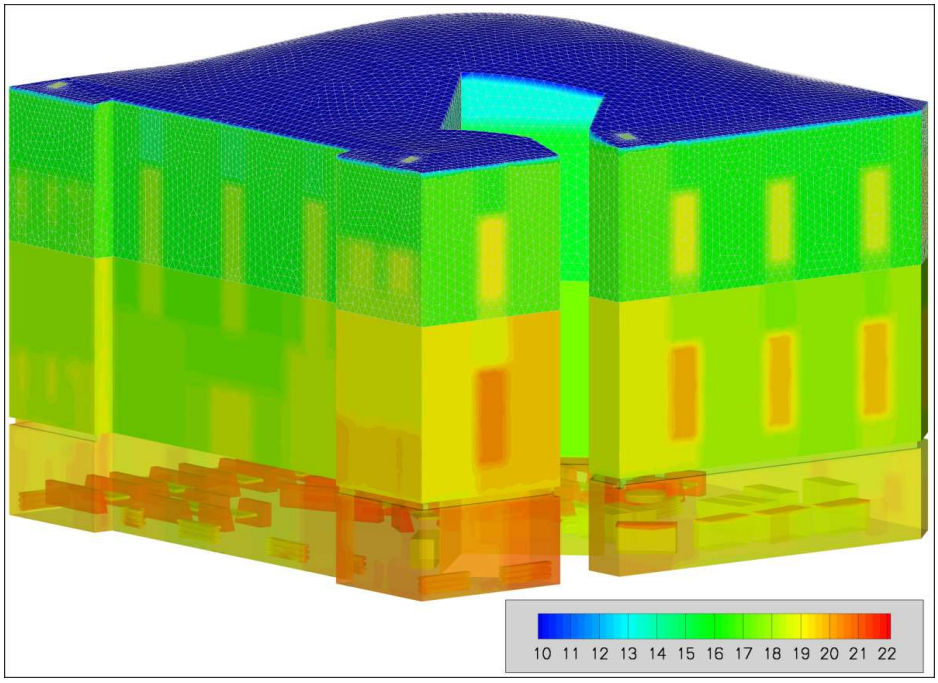

Figure 7. Sketch of the atrium (with cafeteria) with domain decomposition, and boundary conditions for temperature

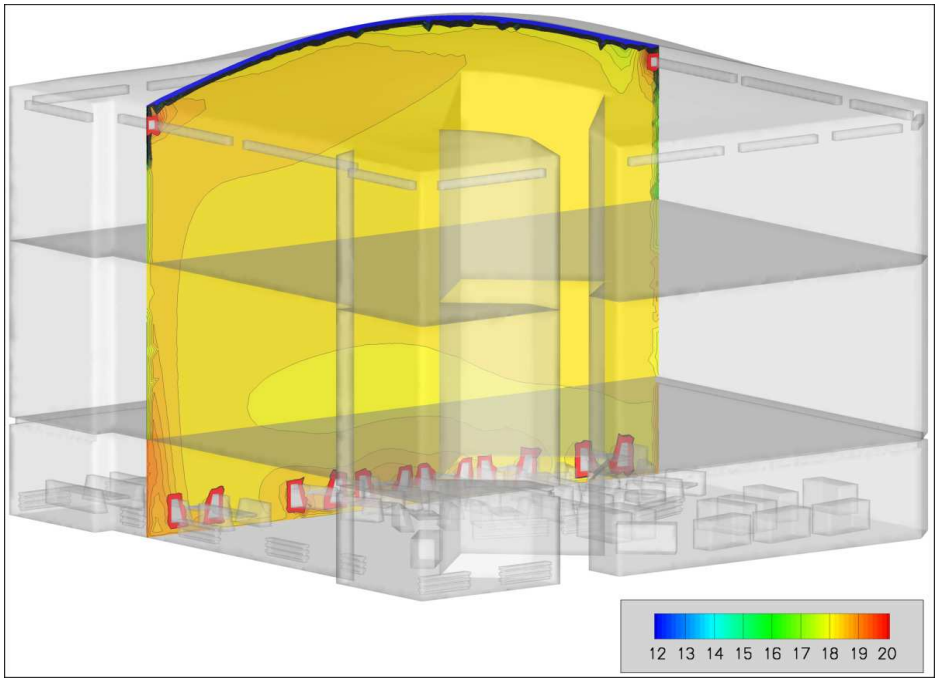

Figure 8. Temperature distribution in a selected cross-section of the atrium

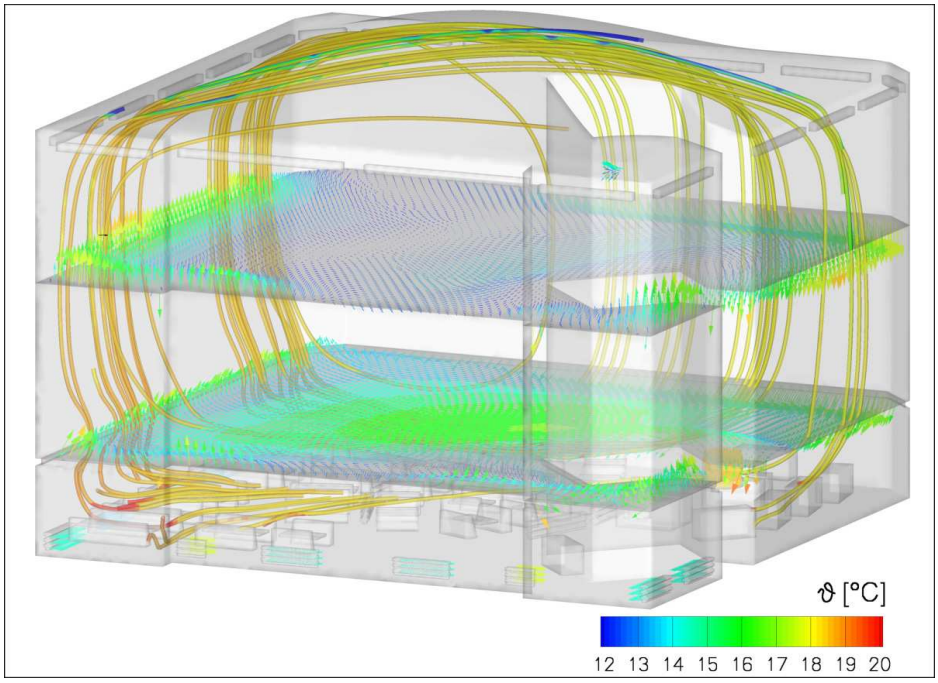

Figure 9. Details of the flow field in selected planes of the atrium